Structural and magnetic properties of NiC_x and NiN_x ($x = 0$ to $\frac{1}{3}$) solid solutions from first-principles calculations

C. M. Fang,[1,2,*] M. H. F. Sluiter,[3] M. A. van Huis,[1,4] and H. W. Zandbergen[1]

[1]*Kavli Institute of Nanoscience, Delft University of Technology, Lorentzweg 1, 2628 CJ Delft, The Netherlands*

[2]*Materials innovation institute (M2i), Mekelweg 2, 2628 CD Delft, The Netherlands*

[3]*Department of Materials Science and Engineering, Delft University of Technology, Mekelweg 2, 2628 CD Delft, The Netherlands*

[4]*Soft Condensed Matter, Debye Institute for Nanomaterials Science, Utrecht University, Princetonplein 5, 3584 CC Utrecht, The Netherlands*

(Received 23 February 2012; revised manuscript received 13 June 2012; published 19 October 2012)

First-principles calculations have been performed for a variety of Ni_3X (X = C, N) phases, as well as for NiX_y ($y = 0$ to $\frac{1}{3}$) solid solutions to clarify the persistent controversy regarding its magnetic state. The calculations show that the solid solution phases based on hexagonal-close-packed (hcp or ε-) Ni have relatively high stability for X concentrations greater than about 0.1 whereas the face-centered-cubic (fcc or γ-) Ni phases are favored for smaller X concentration. Hence, during carburization or nitridization of Ni, a phase transformation is to be expected. In spite of the close-packed nature of both hcp- and fcc-based solid solutions, X quenches the magnetization more effectively in fcc than in hcp-based solid solutions. These findings resolve many apparently contradictory experimental observations concerning C- and N-containing Ni alloys in the literature.

DOI: 10.1103/PhysRevB.86.134114 PACS number(s): 61.50.Lt, 71.20.Be, 75.50.Cc, 31.10.+z

I. INTRODUCTION

Ni_3X (X = C and N) phases have been the subject of scientific investigation due to their potential for industrial applications.[1–12] In recent years, much attention has been paid to different Ni_3X materials, such as nanosized crystallites[3–10] and thin films.[11,12] Ni_3N samples were first prepared by means of nitridation of Ni metal using ammonia.[1,2,13,14] Neklyudov and Morozov prepared nickel nitrides using nitrogen ion implantation and reported two hexagonal phases, α-Ni_3N (a = 2.66 Å and c = 4.30 Å) and β-Ni_3N (a = 4.66 Å, c = 4.30 Å),[15] whereby they claimed N atomic disorder in the α-Ni_3N phase. Leineweber *et al.* studied the order of nitrogen in hexagonal (β-)Ni_3N using neutron diffraction techniques and observed only little disorder (~3 at. %).[16,17] In the literature the crystal structure of Ni_3C is much debated.[1,2,18,19] The early work suggested a hexagonal lattice (a = 2.628 Å and c = 4.308 Å),[2,18] while Goldschmidt considered that Ni_3C probably has the orthorhombic cementite-type structure.[1] Later on, Nagakura determined that it has a rhombohedral lattice ($3R$-) with a = 4.553 Å and c = 12.92 Å.[2,19] Reports of the electronic and magnetic properties of the Ni_3X phases are also contradictory.[6,17,20–24] Choi and Gillan reported that their Ni_3N samples are (ferro)magnetic, being strongly attracted to a permanent magnet,[6,20] but others reported nonmagnetism for both Ni_3N and Ni_3C phases.[7,9,21,22] Recently, Schaefer and co-workers proposed a Ni_3C_{1-x} solid solution to bridge the delimiting hcp-Ni and Ni_3C phases.[5] In fact, there is frequent confusion about the hcp-Ni (Ref. 23) and the hexagonal Ni_3C phases, as pointed out by He.[24]

There are also many theoretical investigations of the Ni_3X phases.[7,20–22,25–28] Shein and co-workers investigated the electronic properties of orthorhombic θ-TM_3C (TM = Fe, Ni) of the cementite-type structure[25] using a first-principles method. Gibson and co-workers explored the structure and stability of nickel carbides, including both hexagonal and orthorhombic Ni_3C phases, and concluded that the hexagonal phase is more stable.[26] Up to now, all theoretical studies have revealed the nonmagnetic nature for the Ni_3N and Ni_3C phases. In the present manuscript, we report the results of first-principles calculations on various Ni_3X (X = C, N) phases, as well as NiX_y ($0 \leqslant y \leqslant \frac{1}{3}$) solid solutions. The relative stability and the structural, electronic, and magnetic properties of these phases are addressed. The information obtained is used to understand the formation, chemical compositions, and stability of the Ni_3X phases and the NiX_y solutions, and to understand the chemical processes such as carburization and nitridation of Ni.[1–3,5,29,30]

II. DETAILS OF METHODS

The first-principles code VASP (Refs. 31 and 32) employing density functional theory (DFT) within the projector-augmented wave (PAW) method[33,34] was used for all the calculations. The generalized gradient approximation (GGA), formulated by Perdew, Burke, and Ernzerhof (PBE),[35] was employed for the exchange and correlation energy terms because the GGA describes spin-polarized transition metals and compounds better than the local-density approximation (LDA).[36,37] The cutoff energy of the wave functions was 550 eV, and the cutoff energies of the augmentation functions were 700 eV for carbides and nitrides. The electronic wave functions were sampled on Γ-centered grids,[38] $16 \times 16 \times 24$, $16 \times 12 \times 16$, and $12 \times 12 \times 16$ in the first Brillouin zone (BZ) of θ-Ni_3X, of $3R$-Ni_3X, and of hcp-Ni_3X_y ($0 \leqslant y \leqslant 1$), respectively. Structural optimizations were performed for both the lattice parameters and atomic coordinates. For the calculation of atom-decomposed electronic configurations and partial density of states, Wigner-Seitz radii of 1.4 Å (Ni) and 1.0 Å (X) were used. The plane waves in the sphere were decomposed into $2s$, $2p$, and $3d$ ($4s$, $4p$, and $3d$) states in the spheres of C/N (Ni) for both spin-up (or majority) and spin-down (minority) direction, respectively. In this way a local magnetic moment is obtained from the difference of the spin-up electrons and spin-down electrons in the sphere.

TABLE I. Calculated results for the Ni phases, compared with the experimental values and previous theoretical calculations.

	fcc-Ni (γ phase)		hcp-Ni (ε phase)	
Method	Lattice parameter (Å)	Magnetic moment (μ_B/Ni)	Lattice parameter (Å)	Magnetic moment (μ_B/Ni)
DFT-GGA (present)	$a = 3.524$	0.626	$a = 2.490$ $c = 4.088$	0.638
DFT-GGA[a]			$a = 2.488$ $c = 4.099$	0.63
DFT-GGA[b]	$a = 3.517$	0.63		
DFT-GGA[c]	$a = 3.52$		$a = 2.49$ $c = 4.09$	
Experiments[d]	$a = 3.524$	~0.60	$a = 2.49$ $c = 4.09$	

[a]Reference 7.
[b]Reference 25.
[c]Reference 26.
[d]References 39–41.

To understand the origin of the nonmagnetism of the Ni compounds, the fixed-spin method was used.[31,32] Tests of k-mesh and cutoff energies showed a good energy convergence (<1 meV/atom).

III. CALCULATED RESULTS AND DISCUSSION

A. The Ni phases

First, the calculations were performed for the face-centered-cubic (fcc, or γ-) and hexagonally close-packed (hcp, ε-) phases of Ni metal. The calculations showed a ferromagnetic ordering with a moment of about 0.63 μ_B per Ni atom for fcc-Ni and 0.64 μ_B per Ni for hcp-Ni (Table I). The calculations reproduced the experimental values as shown in Table I. The calculations also showed that fcc-Ni is the ground state and the energy difference between fcc- and hcp-Ni is about 22.8 meV/atom, in agreement with previous calculations,[7,25,26] and with the observed instability of hcp-Ni at room temperature.[41] The hcp structure differs from the fcc structure only in the stacking of the close-packed atomic planes; the length of the a axis of the hcp lattice can be approximated by $a_{hcp} = a_{fcc}\sqrt{2}/2 = 2.49$ Å and $c_{hcp} = a_{fcc}\sqrt{3}/3 = 4.07$ Å. These approximations are close to the *ab initio* computed dimensions of the hcp unit cell as shown in Table I.

B. Relative stability of the Ni_3X phases

The formation energy $\Delta E(Ni_pC_qN_r)$ per atom of a $Ni_pC_qN_r$ phase is defined with respect to elements Ni (fcc phase), C (graphite), and N (N_2 molecule) as follows:

$$\Delta E(Ni_pC_qN_r) = \{E(Ni_pC_qN_r) - pE(Ni) - qE(C) - rE(N)\}/(p + q + r). \quad (1)$$

The energy for graphite was obtained from the calculated total energy of diamond with a correction of about 17 meV (details in Refs. 42–44). Calculations for the N_2 molecule were performed in a large cube with axis length $a = 12$ Å.[42] The cutoff energy of the wave functions of 1000 eV was employed to describe the strongly localized $2p$ bonds of the N_2 molecule. The calculated bond length is 1.11 Å, comparable to the experimental value (1.10 Å).

The calculated results for the Ni_3X (X = C, N) phases are listed in Table II. Calculations were also performed for the Ni_3X phase with the well-known Cu_3N-type structure, as well as the fcc-Ni_4X phase with the Fe_4N-type structure.[1,2] All the nickel carbides and nitrides have positive formation energies, indicating that they are unstable relative to the elemental phases (fcc-Ni, graphite, and the N_2 molecule). Especially the formation energies for the Ni_3X phases with the Cu_3N type structure and the fcc-Ni_4X phase are very high.

As shown in Table II, the carbide θ-Ni_3C has a formation energy of 73 meV/atom, while the nitride variant θ-Ni_3N has a much higher formation energy of 394 meV/atom. Meanwhile, the phases with hcp-Ni sublattices have much lower formation energies. The calculations also showed an energy difference of about 36.1 meV/atom between θ-Ni_3C and 3R-Ni_3C, close to the recently calculated values (0.14 eV/f.u. or about 35 meV/atom) by Gibson and co-workers[26] and to the values (0.157 eV/f.u. or 39.3 meV/atom) found by Hwang and co-workers.[7]

The calculated length of the a axis for the Ni_3X phases ranges from 4.59 to 4.65 Å, or from 2.65 to 2.68 Å in a simple hcp lattice. These values are about 0.15–0.19 Å larger than that of hcp-Ni. This difference is useful to identify and distinguish the Ni phases and Ni_3X phases in different forms, such as in nanocrystals or in thin films.[6–12,19,23,24]

Both hcp- and 3R-Ni_3X phases have hexagonal close-packed (hcp) Ni sublattices (Fig. 1 and Table II). They differ from each other in the arrangements of X atoms in the octahedral interstitial sites. In hcp-Ni_3X the interstitial planes follow an . . .ABAB. . . stacking, while in 3R-Ni_3X the interstitial planes have an . . .ABCABC. . . stacking. Although the calculations show higher stability for hcp-Ni_3N and 3R-Ni_3C than for 3R-Ni_3N and hcp-Ni_3C, respectively, the energy difference is small (~3 meV/atom) for the carbide, and about 11 meV for the nitride (Table II) as could be expected on the basis of the similarity of the two structure types. Such small energy differences indicate possible coexistence of both phases, or configurational disorder of the interstitial X atoms in hcp-Ni, as found experimentally.[19] The slightly larger energy

TABLE II. Calculated results for the Ni_3X (X = C, N) phases, having orthorhombic (a), hexagonal-close-packed (b), rhombohedral (c) Cu_3N-type (d), and γ'-Fe_4N (e) crystal structures, using the DFT-GGA-PBE method. Experimental values and former calculations are included for comparison.

	Nickel nitrides			Nickel carbides		
Structure and space group	Formula	Lattice parameter (Å)	ΔE meV/atom	Formula	Lattice parameter (Å)	ΔE meV/atom
(a) Orthorhombic *Pnma* (62)	θ-Ni_3N	$a = 4.981$ $b = 7.099$ $c = 4.474$	+293.6	θ-Ni_3C	$a = 4.953$; (4.956)[a] (4.95)[b] $b = 6.800$; (6.809)[a] (6.79)[b] $c = 4.472$; (4.465)[a] (4.43)[b]	+73.4
(b) hcp $P6_322$ (182)	hcp-Ni_3N	$a = 4.625$ (4.6224)[c] (4.66)[d] $c = 4.314$ (4.3059)[c] (4.30)[d]	+32.9	hcp-Ni_3C	$a = 4.591$ $c = 4.348$	+40.7
(c) Rhombohedral R-3c (167)	3R-Ni_3N	$a = 4.652$ $c = 12.919$	+44.0	3R-N_3C	$a = 4.604$ (4.553)[e] (4.60)[f] $c = 13.022$(12.92)[e] (13.016)[f]	+37.3
(d) Cu_3N Pm-3m (221)	Ni_3N	$a = 3.430$	+915.5	Ni_3C	$a = 3.369$	+817.3
(e) γ'-Fe_4N Pm-3m (221)	γ'-Ni_4N	$a = 3.737$ (3.77)[d]	+93.2	γ'-Ni_4C	$a = 3.740$	+199.4

[a]Reference 25.
[b]Reference 26.
[c]Reference 16.
[d]Reference 15.
[e]Reference 19.
[f]Reference 7.

difference between hcp- and 3R-Ni_3N (about 11 meV/atom) indicates that N disorders less readily than C in hcp-Ni, in agreement with the experimental observations.[16,17]

C. Magnetic properties of the Ni compounds

To have a better understanding about the relationships between the magnetism and the thermodynamic stability, we calculated the dependency of the formation energies on the magnetic moment (per Ni or $NiX_{1/3}$) using the fixed magnetic moment approach. The calculated results are shown in Fig. 2. For fcc-Ni, the nonmagnetic solution is very unstable (about 55 meV/Ni). This is understandable because the nonmagnetic solution has a high density of states at the Fermi level. The calculated total energy decreases with increasing magnetic moment for fcc-Ni as the exchange splitting increases. The formation energy reaches the minimum at $M = 0.63$ (μ_B/Ni). Further increase of magnetic moment reduces the occupation of the spin-down states since the spin-up states are occupied. This requires much energy, which destabilizes the structure. On the other hand the nonmagnetic solution is the most stable for both hcp-Ni_3N and 3R-Ni_3C, whereby the total energies increase strongly with increasing magnetic moment (Fig. 2). That is because the Fermi level is at the upper part of the Ni 3d states and a forced exchange splitting will cause electron

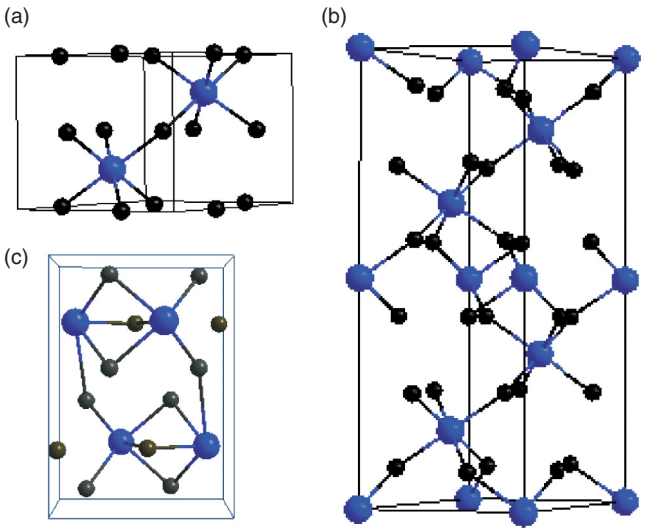

FIG. 1. (Color online) Schematic structures of Ni_3X for the hcp phase (a), 3R phase (b), and θ phase (c).

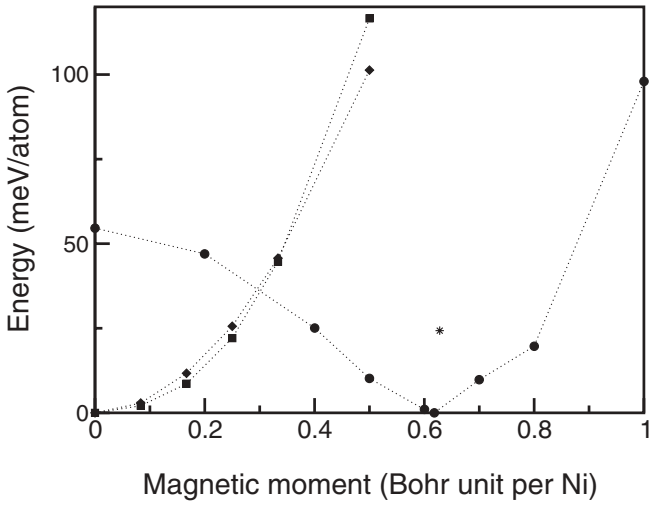

FIG. 2. The relationships between total energy and magnetic moment (i.e., magnetization per Ni atom) for fcc-Ni (●), 3R-Ni_3C (♦), hcp-Ni_3N (■). The energy relative to fcc-Ni and the magnetic moment for hcp-Ni metal (∗) is included for comparison. The energies are displayed with respect to their minimum value.

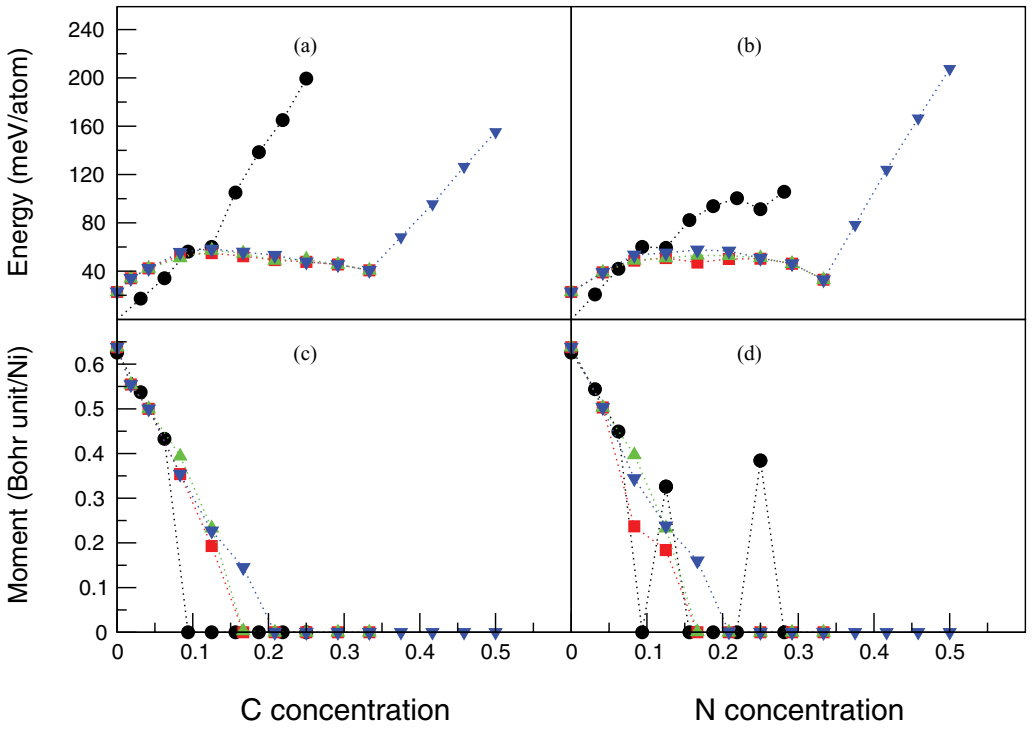

FIG. 3. (Color online) The dependencies of calculated formation energies (a), (b) and magnetic moments (c), (d) on X concentration (y) in the hcp- and fcc-NiX_y solid solutions. The black spheres represent fcc-NiX_y, the red squares hcp-1l, the green upward triangles hcp-2l-close, and the blue downward triangles hcp-2l-far arrangements, as discussed in Sec. III D of the text.

transfer from the Ni $3d$ states to the C/N $2p$ band in the ferromagnetic solution. Such electron transfer is energetically unfavorable. This indicates high stability of the nonmagnetic solution for these phases.

D. The hcp-NiC$_y$ solid solution

Recently the hcp-Ni$_3$C$_x$ or (hcp-NiC$_y$) solid solution was proposed by Schaefer and co-workers[5] to bridge the ε-Ni and ε-Ni$_3$C phases. As shown in Sec. III C, the Ni phases have ferromagnetic ordering. The question now arises of how the magnetism changes with the chemical composition of the phases. The magnetic and structural properties were calculated for hcp- and fcc-NiC$_y$ solid solutions ($y = 0.0$ to $\frac{1}{3}$). Considering the similar formation energies of the hexagonal $3R$-Ni$_3$C and hcp-Ni$_3$C phases, the calculations were performed only for the hcp-Ni$_3$C$_x$ solid solution. A supercell was employed with dimensions $a_h = 2\sqrt{3}a_0, c_h = c_0$ (here a_0 and c_0 are the lattice parameters of a primitive hcp-Ni$_3$C), containing 24 Ni atoms and eight C atoms (we still use the Wyckoff labels from the primitive cell for the supercell). The 24 Ni atoms form an hcp lattice with eight C atoms at the c sites. The eight c sites are positioned equally in two layers. Starting from hcp-Ni, the C ordering in the hcp-NiC$_x$ ($x = 0$ to $\frac{1}{3}$) solution is arranged in three ways: (a) configuration hcp-1l: the C atoms are all in one layer, (b) configuration hcp-2l-far: C atoms are mutually separated as far as possible; (c) configuration hcp-2l-close: the C atoms are arranged in two layers and are as close as possible within that layer. Calculations were also performed for fcc-NiC$_x$ with a $2a_0 \times 2a_0 \times 2a_0$ supercell (a_0 is the lattice parameter of fcc-Ni) containing 32 Ni atoms. The calculated results are shown in Figs. 3 and 4.

We also performed calculations for dilute C/N solution in ε-Ni. For this purpose, a supercell with $a_h = 3a_0$, $c_h = 3c_0$ (here a_0 and c_0 are again the lattice parameters of a primitive hcp-Ni$_3$C cell) containing 54 Ni atoms was employed. The calculations showed that the addition of a C/N atom at an octahedral site of the hcp-Ni lattice costs 0.650 eV (0.766 eV) per C (N) atom. The energy cost reduces to 0.508 eV/X for the smaller supercell with $a_h = 2\sqrt{3}a_0$, $c_h = c_0$, as shown in Fig. 3. Table III lists the calculated formation energies for several defects, including the Ni vacancy, the Ni self-interstitial, and C/N interstitials at the octahedral and tetrahedral sites of fcc-Ni. Details on the configurations and dimensions of the supercells are given in the Supplemental Material[50] (Table S1, Fig. S1. Details on the local magnetic moments on the first- and second-nearest neighbor Ni atoms around the C/N atom are given in Table S2).[50] The calculations (Table III) show that it costs 0.568 (0.628 eV) to insert one C (N) atom at the octahedral site of fcc-Ni. It is also clear from Table III that the formation of vacancies (1.46 eV) is strongly favored over the formation of self-interstitials (3.82 eV).

As shown in Fig. 3, the dependencies of formation energies on C/N concentration are different for the fcc- and hcp-NiX_y systems. For fcc-NiX_y the formation energies increase with increasing X content over the calculated range. The formation energy increases and reaches a maximum at $y \sim 0.10$ for hcp-NiX_y; then it decreases with increasing X concentration. The formation energy for fcc-NiX_y is much lower than that of hcp-NiX_y solution at $y < 0.08$. For values of $y > 0.08$, the formation energy of fcc-NiX_y becomes higher than that of

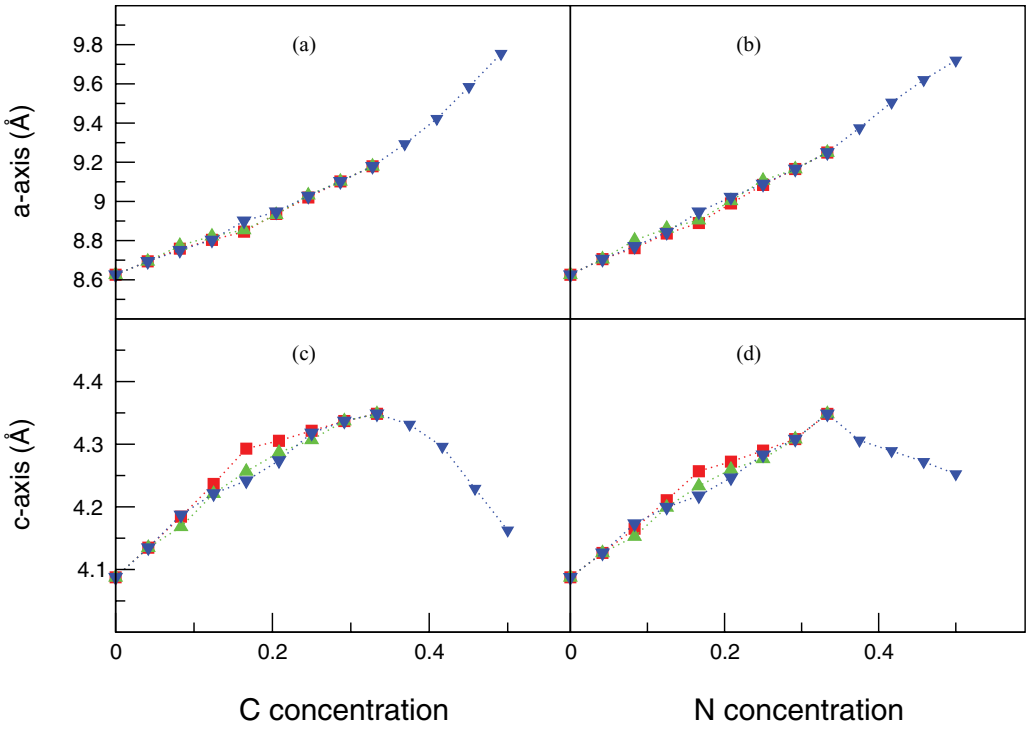

FIG. 4. (Color online) Calculated lattice parameters [a axis (a), (b), c axis (c), (d)] as a function of C/N concentration (y) in the ε-NiX_y solid solution. The squares represent hcp-1l, the upward triangle hcp-2l-close, and the downward triangles hcp-2l-far arrangements.

hcp-NiX_y, the energy difference increasing with x. Therefore, hcp-NiX_y phases become more stable for $y > 0.08$.

In addition, we performed calculations for hcp-NiX_y phases with $y > \frac{1}{3}$. As shown in Fig. 3, the formation energy increases strongly with y in the range between $\frac{1}{3}$ and $\frac{1}{2}$ for both carbides and nitrides. These results differ significantly from the case of iron carbides and iron nitrides, where the formation energy increases moderately with increasing C/N concentrations in this range.[42] Therefore, $y = \frac{1}{3}$ corresponding to the hcp-Ni_3X (X = C, N) phases can be considered as the upper limit of the solid solutions.

Figure 3 also shows the magnetization of the fcc- and hcp-NiX_y systems. For fcc-NiX_y the magnetic moments decrease with X addition, and are quenched for y at 0.08. For hcp-NiX_y solutions, the calculated magnetic moment decreases with increasing X concentrations for all the configurations also, but the magnetization is quenched at much larger fractions X, when x reaches 0.16–0.20. On the other hand, for the NiN_y solutions there are some exceptions: for fcc-$NiN_{0.125}$ and fcc-$NiN_{0.25}$ where the Ni sublattices exhibit little distortion from the fcc lattice, the solutions have significant local magnetic moments (Fig. 3). However, for the latter composition, the formation energy is notably higher than the corresponding hcp structures. Figure 4 shows the relationships between the lattice parameters and C/N concentration of the hcp-NiX_y solution. The lengths of both the a and c parameters increase with increasing X concentration, whereby the c parameter has somewhat larger values for the one-layer X arrangements. However, for the hcp-NiX_y solution with $y > \frac{1}{3}$, the c parameters decrease with increasing C/N concentrations.

TABLE III. DFT-GGA calculations for the self-vacancy, self-interstitial defects and extrinsic C and N atoms at tetrahedral and octahedral sites in fcc-Ni. The values between brackets are from Ref. 49. Details on the configurations and dimensions of the supercells are given in the Supplemental Material (Table S1, Fig. S1) (Ref. 50). Details on the local magnetic moments on the first- and second-nearest neighbor Ni atoms around the C/N atom are given in Table S2 (Ref. 50).

Defect type	Defect energy (eV)
Vacancy	1.46 (1.30–1.80)
Ni (self-) interstitial	3.821
C (octa)	0.568
C (tetra)	2.266
N (octa)	0.682
N (tetra)	1.715

The present calculations show that the nickel carbides hcp-NiC_y are metastable at ambient conditions. In the phase diagram, Singleton and Nash[45] proposed in 1989 a metastable hcp-Ni_3C phase, without discussing its range of formation. Therefore, our calculations agree with the experimental models and furthermore provide a formation range for hcp-NiC_y ($y \leqslant \frac{1}{3}$). There have been investigations on the Ni-N phase diagram also.[46,47] Wriedt reported a metastable fcc-Ni_4N and a stable hcp-Ni_3N in the nickel-rich range. Guillermet and Frisk studied the thermodynamics and stability of the phases in the Ni-N system and proposed stable hcp-NiN_y phases with a formation range for $y \leqslant \frac{1}{3}$. The lower N concentration varies from about $y = 0.15$ at $T \sim 1700$ K to about $y = 0.25$ at $T = 400$ K. In agreement with Guillermet and Frisk's proposal, our calculations show a composition limit with $y \leqslant \frac{1}{3}$.[47] The present calculations also show positive formation energies for

the hcp-NiN_y phases relative to fcc-Ni and N_2 for $T = 0$ K, in contrast to the assessed phase diagram.[47] However, it can be expected that the formation range of the hcp-NiN_y in the assessed phase diagram decreases strongly with decreasing temperature, probably due to the vibrational contributions of N_2 molecules. To have complete knowledge about the stability of the hcp-NiN_y phases at elevated temperature, a full thermodynamical analysis, including lattice vibration (zero-point vibration), magnetic ordering (Curie-Weiss transition), and electronic contributions, is required as shown in Ref. 43. Such an extensive study is beyond the scope of the present work.

From the calculations, we suggest a mechanism of carburization of Ni metals. At elevated temperature, C atoms obtained from decomposition of CO or from graphite move into the octahedral sites of the fcc-Ni metal. With increasing C concentration, the formation energy of fcc-NiC_y increases. When the local C concentration becomes sufficiently large (approximately at $y = 0.08$), fcc-NiC_y transforms into hcp-NiC_y. The stability of hcp-NiC_y increases with increasing C concentration until $y = \frac{1}{3}$, whereby the composition hcp-Ni_3C is formed. The chemical composition of the hcp-NiC_y solution can be estimated by the almost linear relationship between the a- and c-lattice parameters and the C concentration as shown in Fig. 4. In principle, the nitridization process is similar to that of the carburization of Ni metal, due to their similar role in transition metal carbides/nitrides as shown recently for Fe_2X (X = C, N) phases.[48]

IV. SUMMARY

By means of first-principles calculations, the stability, the crystal structure, and the electronic and magnetic properties of various Ni_3X (X = C, N) phases and the related fcc and hcp solid solutions are studied. The calculations showed that hcp-Ni_3C and $3R$-Ni_3C are almost degenerate in energy with the latter slightly favored. In contrast, hcp-Ni_3N is more stable than the $3R$ phase. The magnetism of Ni metals is reduced by the addition of C/N atoms because of strong Ni $3d/X$ $2p$ hybridization. The calculations also show that for NiC_y solutions, the fcc form is more stable at lower C concentrations ($y < 0.06$) while the hcp form becomes much more stable at $y > 0.08$. The formation energies of hcp-NiX_y are rather insensitive to the particular ordering of X atoms. The hcp-NiX_y solid solutions remain ferromagnetic up to $y \sim 0.20$. Both a and c lattice parameters were shown to increase with y in hcp-NiX_y.

*Corresponding address: Kavli Institute of Nanoscience, Delft University of Technology, Lorentzweg 1, NL 2628 CJ Delft, The Netherlands; C.Fang@tudelft.nl

[1] H. J. Goldschmidt, J. Iron Steel Inst. **160**, 345 (1948).
[2] S. Nagakura and S. Oketani, Trans. Iron Steel Inst. Jpn. **8**, 265 (1968).
[3] F. Gillot, J. Oró-Solé, and M. R. Palcín, J. Mater. Chem. **21**, 9997 (2011).
[4] Z. F. Li, R. G. Gordon, V. Pallem, H. Z. Li, and D. V. Shenai, Chem. Mater. **22**, 3060 (2010).
[5] Z. L. Schaefer, K. M. Weeber, R. Misra, P. Schiffer, and R. E. Schaak, Chem. Mater. **23**, 2475 (2011).
[6] J. Choi and E. G. Gillan, Inorg. Chem. **48**, 4470 (2009).
[7] J. Y. Hwang, A. R. P. Singh, M. Chaudhari, J. Tiley, Y. T. Zhu, J. C. Du, and R. Banerjee, J. Phys. Chem. C **114**, 10424 (2010).
[8] P. Hooker, B. J. Tan, K. J. Klabunde, and S. Suib, Chem. Mater. **3**, 947 (1991).
[9] B. Ghosh, H. Dutta, and S. K. Pradhan, J. Alloys Compd. **479**, 193 (2009).
[10] D. L. Leslie-Pelecky, X. Q. Zhang, S. H. Kim, M. Bonder, and R. D. Rieke, Chem. Mater. **10**, 164 (1998).
[11] D. Vampaire, F. Fettar, L. Ortega, F. Pierre, S. Miraglia, A. Sulprice, J. Pelletier, E. K. Hlil, and D. Fruchart, Appl. Phys. Lett. **106**, 073911 (2009).
[12] G. J. W. R. Dorman and M. Sikkens, Thin Solid Films **105**, 251 (1983).
[13] R. Juza and W. Z. Sachsze, Z. Anorg. Allg. Chem. **251**, 201 (1943).
[14] G. W. Watt and D. D. Davies, J. Am. Chem. Soc. **70**, 3753 (1948).
[15] I. M. Neklyudov and A. N. Morozov, Physica B **350**, 325 (2004).
[16] A. Leineweber, H. Jacobs, and S. Hull, Inorg. Chem. **40**, 5818 (2001).
[17] A. Leineweber, H. Jacobs, W. Kockelmann, S. Hull, and D. Hinz-Hübner, J. Alloys Compd. **384**, 1 (2004).
[18] B. Jacobson and A. Westgren, Z. Phys. Chem. B **20**, 361 (1933).
[19] S. Nagakura, J. Phys. Soc. Jpn. **13**, 1005 (1958).
[20] N. S. Gajbhiye, R. S. Ningthoujam, and J. Weissmüller, Phys. Status Solidi A **189**, 691 (2002).
[21] P. Blaha, K. Schwartz, P. Sorantin, and S. B. Trickey, Comput. Phys. Commun. **59**, 399 (1990).
[22] L. Yue, R. Sabiryanova, E. M. Kirkpatrick, and D. L. Leslie-Pelecky, Phys. Rev. B **62**, 8969 (2000).
[23] M. Han, Q. Liu, J. H. He, Y. Song, Z. Xu, and J. M. Zhu, Adv. Mater. **19**, 1096 (2007).
[24] L. He, J. Magn. Magn. Mater. **322**, 1991 (2010).
[25] I. R. Shein, N. I. Medvedeva, and A. L. Ivanovskii, Physica B **371**, 126 (2006).
[26] J. S. Gibson, J. Uddin, T. R. Cundari, N. K. Bodiford, and A. K. Wilson, J. Phys.: Condens. Matter **22**, 445503 (2010).
[27] L. Lu, M. L. Sui, and K. Lu, Science **287**, 1463 (2000).
[28] W. P. Tong, N. R. Tao, Z. B. J. Lu, and K. Lu, Science **299**, 686 (2003).
[29] H. J. Grabke, Corrosion **56**, 801 (2000).
[30] S. Simonetti, L. Moro, G. Brizuela, and A. Juan, J. Phys. D: Appl. Phys. **41**, 125006 (2008).
[31] G. Kresse and J. Hafner, Phys. Rev. B **47**, 558 (1993).
[32] G. Kresse and J. Furthmüller, Comput. Mater. Sci. **6**, 15 (1996).
[33] P. E. Blöchl, Phys. Rev. B **50**, 17953 (1994).
[34] G. Kresse and D. Joubert, Phys. Rev. B **59**, 1758 (1999).
[35] J. P. Perdew, K. Burke, and M. Ernzerhof, Phys. Rev. Lett. **77**, 3865 (1996).
[36] C. Amador, W. R. L. Lambrecht, and B. Segall, Phys. Rev. B **46**, 1870 (1992).
[37] C. M. Fang, M. A. van Huis, M. H. F. Sluiter, and H. W. Zandbergen, Acta Mater. **58**, 2968 (2010).

[38]H. J. Monkhorst and J. D. Pack, Phys. Rev. B **13**, 5188 (1976).
[39]R. Wyckoff, *Crystal Structures* (Interscience, New York, 1964).
[40]A. Hemenger and H. Weik, Acta Crystallogr. **19**, 690 (1965).
[41]J. G. Wright and J. Goddard, Philos. Mag. **11**, 485 (1965).
[42]C. M. Fang, M. A. van Huis, and H. W. Zandbergen, Scr. Mater. **64**, 296 (2011).
[43]C. M. Fang, M. H. F. Sluiter, M. A. van Huis, C. K. Ande, and H. W. Zandbergen, Phys. Rev. Lett. **105**, 055503 (2010).
[44]C. M. Fang, M. A. van Huis, and H. W. Zandbergen, Phys. Rev. B **80**, 224108 (2009).
[45]M. Singleton and P. Nash, Bull. Alloy Phase Diagrams **10**, 121 (1989).
[46]H. A. Wriedt, Bull. Alloy Phase Diagrams **6**, 558 (1985).
[47]A. F. Guillermet and K. Frisk, Int. J. Thermophys. **12**, 417 (1991).
[48]C. M. Fang, M. A. van Huis, J. Jansen, and H. W. Zandbergen, Phys. Rev. B **84**, 094102 (2011).
[49]Y. Kraftmakher, Phys. Rep. **299**, 79 (1998).
[50]See Supplemental Material at http://link.aps.org/supplemental/10.1103/PhysRevB.86.134114 for details on the supercells and local magnetic moments.